ACS OMEGA

http://pubs.acs.org/journal/acsodf

Article

Water Adsorption Behavior on a Highly Dense Single-Walled Carbon Nanotube Film with an Enhanced Interstitial Space

Dong Young Kim,* Keun Soo Kim, Cheol-Min Yang, and Jungpil Kim*

Cite This: *ACS Omega* 2021, 6, 7015−7022

Read Online

ACCESS | Metrics & More | Article Recommendations

ABSTRACT: In this study, we describe the adsorption behavior of water (H_2O) in the interstitial space of single-walled carbon nanotubes (SWCNTs). A highly dense SWCNT (HD-SWCNT) film with a remarkably enhanced interstitial space was fabricated through mild HNO_3/H_2SO_4 treatment. The N_2, CO_2, and H_2 adsorption isotherm results indicated remarkably developed micropore volumes (from 0.10 to 0.40 mL g^{-1}) and narrower micropore widths (from 1.5 to 0.9 nm) following mild HNO_3/H_2SO_4 treatment, suggesting that the interstitial space was increased from the initial densely-packed network assembly structure of the SWCNTs. The H_2O adsorption isotherm of the HD-SWCNT film at 303 K showed an increase in H_2O adsorption (i.e., by ∼170%), which increased rapidly from the critical value of relative pressure (i.e., 0.3). Despite the remarkably enhanced adsorption capacity of H_2O, the rates of H_2O adsorption and desorption in the interstitial space did not change. This result shows an adsorption behavior different from that of the fast transport of H_2O molecules in the internal space of the SWCNTs. In addition, the adsorption capacities of N_2, CO_2, H_2, and H_2O molecules in the interstitial space of the HD-SWCNT film showed a linear relationship with the kinetic diameter, indicating an adsorption behavior that is highly dependent on the kinetic diameter.

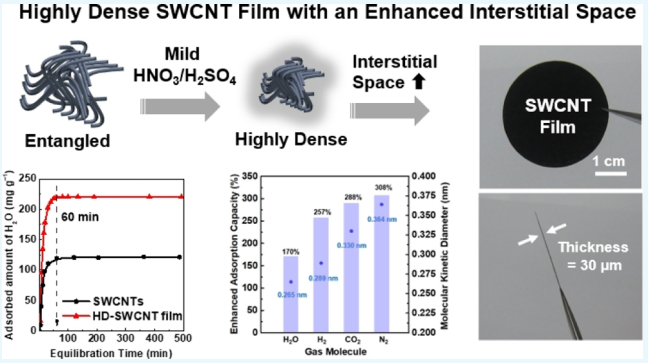

INTRODUCTION

Water (H_2O) adsorption into porous materials, such as porous silica, metal−organic frameworks, and metal-based catalyst materials, has been studied passionately over a number of years because of its potential applicability in eco-friendly energy devices.[1−6] In addition, studies into the adsorption/desorption of H_2O molecules in these nanoporous materials have been the basis for energy and environmental research in industrial processes, such as H_2O purification, desalination, drug delivery, and ion transport.[7−10] Since the adsorption/desorption behaviors of H_2O molecules are altered by the pore structures and properties of such materials, further research is required in this area.

Carbon nanoporous materials mainly possess a hydrophobic surface but show a unique phenomenon in which the adsorption of H_2O molecules increases rapidly at a critical value of the relative H_2O vapor pressure.[11−14] The adsorption of H_2O through control of the pore structures of these nanoporous carbons has been extensively studied.[15−17] For example, the mechanisms for stable H_2O cluster formation and adsorption in nanoporous carbons with different pore widths were examined through small-angle X-ray scattering measurements, simulations, and in situ molecular adsorption studies for carbon materials with nanopores of various shapes (i.e., activated carbon fibers, carbon nanohorns, and carbon aerosol materials).[18−20]

Single-walled carbon nanotubes (SWCNTs) with one-dimensional hollow structures and high aspect ratios can be divided into their internal spaces and interstitial spaces, which are formed by the networks between the nanotube bundles.[21,22] In particular, the narrow internal spaces of SWCNTs with diameters of generally ≤2 nm can realize the fast transport of molecules (e.g., H_2O) with a particularly strong confinement effect.[23−27] In this context, Holt et al. reported a mechanism for the fast transport of H_2O to microfabricated membranes using sub-2 nm SWCNT arrays.[24] In addition, Tunuguntla et al. reported an enhanced H_2O permeability and tunable ion selectivity through the application of 0.8 nm diameter SWCNT porins,[27] while Ohba et al. studied the formation of H_2O clusters in the SWCNT internal space and examined the H_2O adsorption mechanism based on

Received: December 28, 2020
Accepted: February 18, 2021
Published: March 2, 2021

the nanotube diameter using X-ray diffraction and molecular simulation analyses.[28,29] Furthermore, a number of studies into the unique H_2O adsorption phenomena and mechanisms taking place in the SWCNT internal spaces have been reported.[30−32]

However, compared to extensive and systematic studies into the internal spaces of SWCNTs, studies into the adsorption behaviors and storage mechanisms of molecules, such as H_2O, in the interstitial spaces of SWCNTs are rare. The interstitial space formed by the assembly network between nanotubes has the advantage of being able to freely control the nanoporosity through interfacial engineering of a solution-based process, unlike the internal space determined by the nanotube diameter.[33−38] The study of H_2O adsorption in such developed interstitial spaces would therefore be expected to provide a clear understanding of the nanoporous structures of SWCNTs and the adsorption behaviors of different molecules.

Thus, we herein report the behavior of H_2O adsorption in the interstitial spaces of SWCNTs, which are remarkably developed through mild acid treatment. The rates of H_2O adsorption and desorption are examined before and after the treatment, and the adsorption capacity of the molecule, which depends on the kinetic diameter of the molecule, is also described.

RESULTS AND DISCUSSION

Figure 1a,b shows photographic images of the highly dense SWCNT (HD-SWCNT) film fabricated via mild acid treatment in HNO_3/H_2SO_4 at 298 K and subsequent vacuum filtration (VF). The HD-SWCNT film exhibits a relatively uniform and rigid surface, and the film thickness was determined to be ∼30 μm. Figure 1c,d shows the field emission scanning electron microscopy (FE-SEM) images of the surface morphologies of the SWCNTs and the HD-SWCNT film, respectively. After HNO_3/H_2SO_4 treatment, the network assembly form of the HD-SWCNT film exhibited a fairly uniform and dense structure (Figure 1d). The dense packing structure of the HD-SWCNT film can be attributed to the following two phenomena: (1) randomly entangled as-grown SWCNT bundles are highly dispersed by oxygen-containing functional groups introduced by the HNO_3/H_2SO_4 treatment, and (2) the individual SWCNTs in the dispersed suspension are densely rearranged through the VF process after sonication. The assembly of SWCNTs through a high dispersion and rearrangement process by the introduction of oxygen-containing functional groups is therefore a simple and effective method for controlling the narrow microporosity in solution-based CNT processes. Such a dense assembly structure of the HD-SWCNT film can provide a remarkably developed adsorption capacity attributed to increasingly narrow micropores.

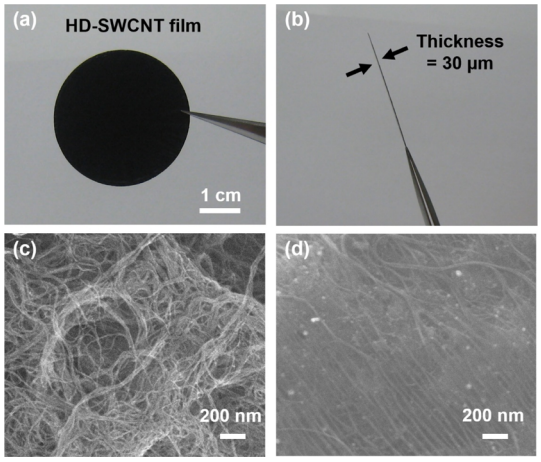

Figure 1. (a,b) Photographic images of the HD-SWCNT film fabricated using the mild HNO_3/H_2SO_4 treatment process, and FE-SEM images of the (c) SWCNTs and (d) HD-SWCNT film.

To determine the surface chemical states of the SWCNTs and the HD-SWCNT film, X-ray photoelectron spectroscopy (XPS) was carried out (Figure 2). The C 1s spectra were fitted with four peaks originating from C═C and/or C−H (284.4 eV), C−O and/or C═O (286.4 eV), O−C═O (288.6 eV), and $\pi-\pi^*$ shake-up (290.4 eV), as shown in Figure 2a,b.[39,40] After functionalizing the SWCNTs by HNO_3/H_2SO_4 treatment and thermal treatment at 1173 K (HD-SWCNT film), the content of the oxygen-containing functional groups (i.e., C−O and/or C═O) increased by up to 42.4% (Figure 2a,b). Recently, our group demonstrated the peak shifts and the corresponding full widths at half-maximum (fwhms) of the XPS peaks of nanocarbon materials with various defects.[39,41−43] The XPS peak originating from vacancy defects appears at ±0.7 eV from the C═C and/or C−H main peak.[39,41] Thus, the fwhm of the peak originating from the C═C and/or C−H peak increased upon the introduction of internal pores to the CNT wall due to the presence of an increased number of vacancies and edge structures in the wall.[39,41] However, the fwhm of the peak originating from the C═C and/or C−H moiety of the HD-SWCNT film was not increased compared to that of the SWCNTs (Figure 2c), which indicates either that the number of internal pores was small or that no internal pores were introduced.

In Figure 3a, the adsorption isotherms of the SWCNTs are typical IUPAC type II isotherms, whereas the HD-SWCNT film was found to exhibit a type IV isotherm with small hysteresis, especially in the low relative pressure region (P/P_0 = 0.1). In addition, the film presented a significantly higher adsorption capacity (∼2×) than the SWCNTs. In the low relative pressure region (P/P_0 = 0.1), the marked increase in the amount of N_2 adsorption was associated with the development of narrow micropores, which can be more clearly observed in the adsorption isotherm by plotting the logarithm of P/P_0 (see the inset of Figure 3a). The development of this remarkable microporosity can lead to a high micropore surface area and a high micropore volume. The subtracting pore effect (SPE) method determined by the α_s-plots is an effective analytical tool for accurately characterizing micropores.[33,44] Figure 3b shows high-resolution α_s-plots of the adsorption of N_2 by the SWCNTs and the HD-SWCNT film. A significant increase in the lower regions of the α_s-plots ($\alpha_s < 0.5$) indicates the presence of abundantly developed uniform micropores. The pore structure parameters of the SWCNTs and the HD-SWCNT film calculated from the SPE method are summarized in Table 1. After HNO_3/H_2SO_4 treatment, the total surface area of the HD-SWCNT film increased approximately 3 times from 341 to 1048 $m^2\ g^{-1}$, as shown in Table 1 and Figure 3c. This significant increase in the total surface area is mainly due to the increased interstitial space between nanotubes, which in turn is caused by the formation of tightly packed assembly structures. The micropore surface area of the HD-SWCNT film increased by approximately 10 times from 82 to 859 m^2

https://dx.doi.org/10.1021/acsomega.0c06302
ACS Omega 2021, 6, 7015−7022

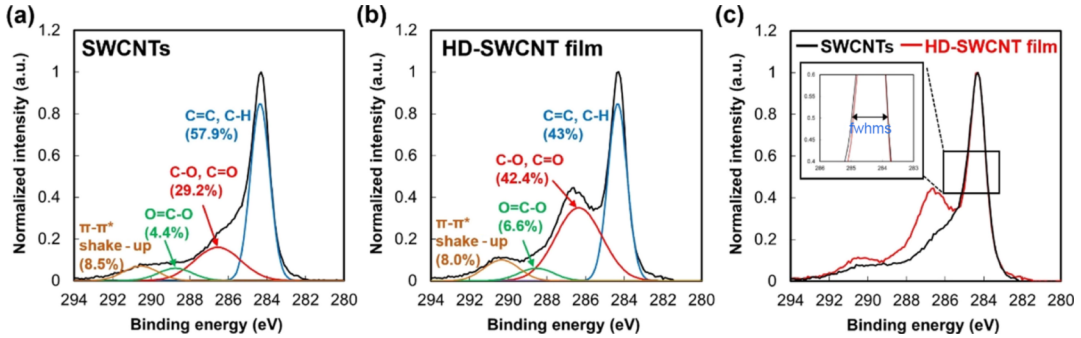

Figure 2. C 1s XPS spectra of the SWCNTs and the HD-SWCNT film. (a) Peak separation of the SWCNTs. (b) Peak separation of the HD-SWCNT film. (c) Comparison of the fwhms of the peaks originating from the C═C and C−H moieties between the SWCNTs and the HD-SWCNT film.

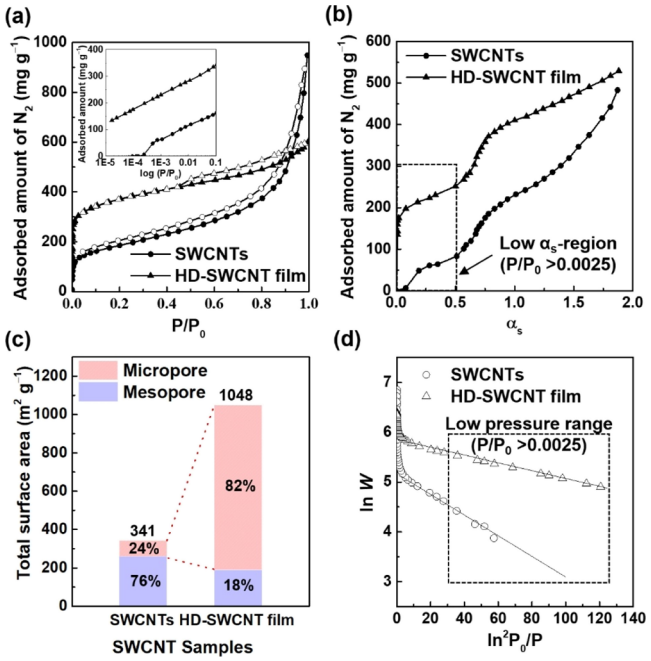

Figure 3. N_2 adsorption properties of the SWCNT samples at 77 K. (a) N_2 adsorption isotherms of the SWCNTs (●) and the HD-SWCNT film (▲). The solid and open symbols indicate the adsorption and desorption branches, respectively. The inset shows N_2 adsorption isotherms in the logarithmic scale. (b) α_s-plots, (c) Total surface areas, and (d) DR plots of the N_2 adsorption isotherms.

g^{-1}, and the micropore volume increased by 4 times from 0.10 to 0.40 mL g^{-1} (Table 1).

The Dubinin−Radushkevich (DR) equation was then applied to analyze the precise microporous structure and the isosteric heat of adsorption ($q_{st,\Phi=1/e}$) for the SWCNTs and the HD-SWCNT film.[34] Figure 3d shows the DR plot of the N_2 adsorption isotherm at 77 K, where it is apparent that both DR plots of the SWCNTs and HD-SWCNT film are linear in the low-pressure range. The values of $q_{st,\Phi=1/e}$, w, $W_0^{N_2}$, and $W_0^{CO_2}$ obtained from the DR plots are summarized in Table 2. In addition, the average micropore width of the HD-SWCNT film

Table 2. Isosteric Heats of Adsorption ($q_{st,\Phi=1/e}$), Average Micropore Widths (w), and Micropore Volumes ($W_0^{N_2}$ and $W_0^{CO_2}$) Determined from DR Plots of the N_2 (77 K) and CO_2 (273 K) Adsorption Isotherms

sample	$q_{st,\Phi=1/e}$ (kJ mol^{-1})	w (nm)	$W_0^{N_2}$ (mL g^{-1})	$W_0^{CO_2}$ (mL g^{-1})
SWCNTs	9.8	1.5	0.10	0.08
HD-SWCNT films	12.9	0.9	0.40	0.32

was found to narrow from 1.5 to 0.9 nm (Table 2). In general, the $q_{st,\Phi=1/e}$ value depends on the micropore width, the chemical state, and the interaction of the pore walls.[34] This implies that the higher the $q_{st,\Phi=1/e}$ value, the stronger the adsorbent−pore interaction. Following mild HNO_3/H_2SO_4 treatment, the $q_{st,\Phi=1/e}$ value of the HD-SWCNT film increased by 3.1 kJ mol^{-1} compared to that of the SWCNTs. These results clearly indicate the remarkable development of micropores with a narrow average width of 0.9 nm, mainly owing to the enhancement of the interstitial space caused by the formation of highly packed SWCNT assemblies.

Subsequently, the enriched narrow interstitial space of the HD-SWCNT film with w = 0.9 nm was analyzed by applying the CO_2 adsorption technology. Since CO_2 molecules (kinetic diameter = 0.330 nm) are smaller than N_2 molecules (kinetic diameter = 0.364 nm) and have a higher kinetic energy, they can easily access the very narrow interstitial spaces of the nanotubes where N_2 molecules cannot be adsorbed (Table 3).[45,46] Figure 4 shows the CO_2 adsorption isotherms of the

Table 3. Kinetic Diameters of the N_2, CO_2, H_2, and H_2O Molecules

molecule	N_2	CO_2	H_2	H_2O
kinetic diameter (nm)	0.364[45]	0.330[45]	0.289[45]	0.265[46]

Table 1. Pore Structure Parameters of the SWCNTs and the HD-SWCNT Film Determined by the SPE Method

sample	total surface area (m^2 g^{-1})	micropore surface area (m^2 g^{-1})	mesopore surface area (m^2 g^{-1})	total pore volume (mL g^{-1})	micropore volume (mL g^{-1})	mesopore volume (mL g^{-1})
SWCNTs	341	82	259	1.01	0.10	0.91
HD-SWCNT film	1048	859	189	0.72	0.40	0.32

https://dx.doi.org/10.1021/acsomega.0c06302
ACS Omega 2021, 6, 7015−7022

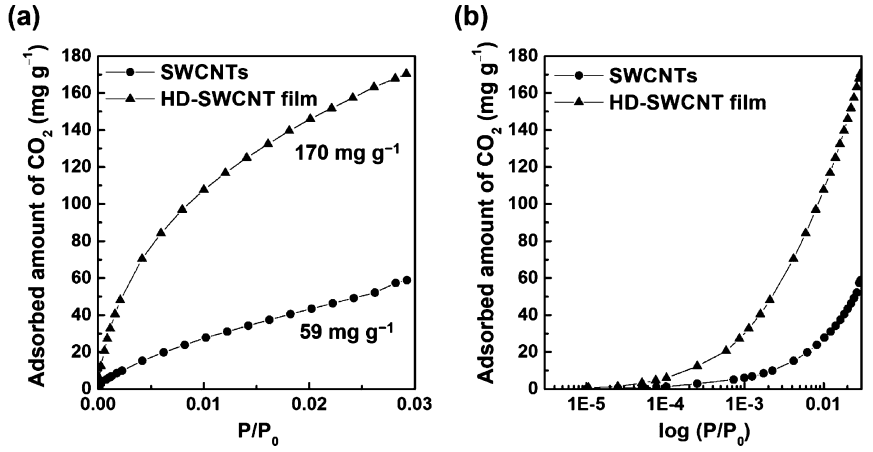

Figure 4. CO_2 adsorption on the SWCNTs and the HD-SWCNT film at 273 K. (a) CO_2 adsorption isotherms and (b) CO_2 adsorption isotherms in the logarithmic scale.

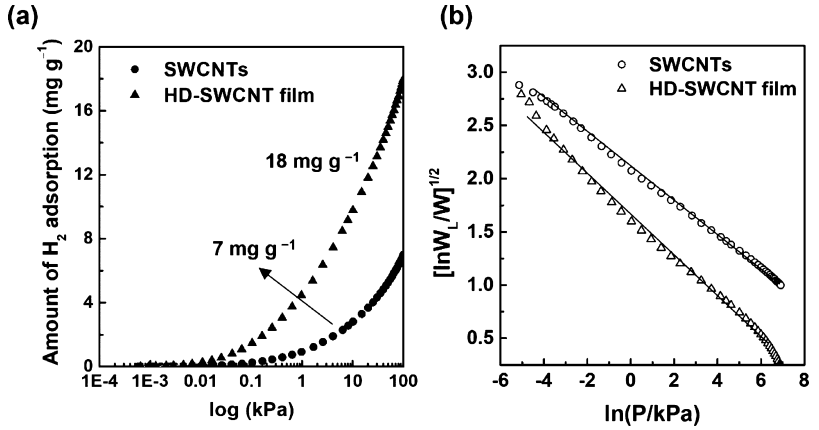

Figure 5. H_2 adsorption on the SWCNTs and the HD-SWCNT film at 77 K: (a) adsorption amount of H_2 and (b) DR plot of the H_2 adsorption isotherm.

SWCNTs and the HD-SWCNT film at 273 K up to a maximum relative pressure (P/P_0) of 0.029. CO_2 adsorption by the HD-SWCNT (170 mg g^{-1}) film exhibits a Langmuir isotherm, in addition to an approximately 2.9 times higher adsorption than the SWCNTs (59 mg g^{-1}). The significant increase in the amount of CO_2 adsorption following HNO_3/H_2SO_4 treatment indicates the presence of well-developed and abundant micropores with a narrow size distribution. After HNO_3/H_2SO_4 treatment, the micropore volume ($W_0^{CO_2}$) value obtained from the DR plot of the CO_2 adsorption isotherm also increased approximately 4 times from 0.32 to 0.08 mL g^{-1}, as outlined in Table 2.

The kinetic diameter of the H_2 molecule is 0.289 nm, which is smaller than that of the CO_2 molecule (0.330 nm), and so can provide accurate information regarding the narrow microporosity of a densely-packed HD-SWCNT film (Table 3). Figure 5 shows the H_2 adsorption isotherm and the DR plot analysis of the SWCNTs and the HD-SWCNT film obtained by H_2 adsorption at 77 K, respectively. In the H_2 adsorption isotherm at a pressure up to 100 kPa, H_2 adsorption by the HD-SWCNT film increased approximately 2.5 times from 7 to 18 mg g^{-1} (Figure 5a). This enhancement in the H_2 adsorption may be associated with an increase in the narrow interstitial space in the SWCNT assembly network following HNO_3/H_2SO_4 treatment. Supercritical DR plots are primarily used to accurately characterize the interactions of micropores with supercritical gases such as H_2. The following supercritical DR equation was therefore applied to analyze the precise microporous structure and the isosteric heat of adsorption for the HD-SWCNT film with an enhanced narrow interstitial space[47−49]

$$[\ln(W_L/W)_{1/2} = (RT/\beta E_0)(\ln P_{0q} - \ln P) \quad (1)$$

where W_L is the amount of saturated H_2 adsorption at 77 K, which can be calculated from the Langmuir plot of the H_2 adsorption isotherm, W is the amount of gas adsorption at adsorption pressure P, P_{0q} is the quasi-saturated vapor pressure, R is the gas constant, and T is the temperature. In addition, β is the affinity coefficient, and E_0 is the characteristic adsorption energy. The isosteric heat of adsorption at the filling ratio of $1/e$, $q_{st,\Phi=1/e}$ can be obtained from the value βE_0 determined from eq 2

$$q_{st,\phi=1/e} = \Delta H_v + \beta E_0 \quad (2)$$

where ΔH_v is the enthalpy of vaporization (ΔH_v of H_2 = 0.898 kJ mol^{-1}). Figure 5b shows the DR plot of a linear H_2 adsorption isotherm at 77 K above 10^{-2} kPa. The measured values of W_L, P_{0q}, and $q_{st,\Phi=1/e}$ are listed in Table 4. As indicated, the W_L and P_{0q} values of the HD-SWCNT film more than doubled, while the $q_{st,\Phi=1/e}$ value for the H_2 molecule gave almost similar values in the range of 4.5−4.6 kJ mol^{-1}. The

https://dx.doi.org/10.1021/acsomega.0c06302
ACS Omega 2021, 6, 7015−7022

Table 4. Adsorption Parameters Calculated by the Supercritical DR Plots of H_2 (77 K) Adsorption

sample	$W_L^{H_2}$ (mL g^{-1})	P_{0q} (kPa) (mL g^{-1})	$q_{st,\Phi=1/e}$ (kJ mol^{-1})
SWCNTs	7.8	$3.9 \times 10^3 \pm 0.4 \times 10^3$	4.6 ± 0.2
HD-SWCNT film	18.9	$1.8 \times 10^3 \pm 0.4 \times 10^3$	4.5 ± 0.2

$q_{st,\Phi=1/e}$ value of the HD-SWCNT film remained relatively unchanged compared to the corresponding value for the SWCNTs, suggesting that the interstitial space following mild HNO_3/H_2SO_4 treatment was similar to that of the SWCNTs. Therefore, this result indicates that the increase in the adsorption amount of H_2 is due to the development of a narrow interstitial space in the HD-SWCNT film.

The SWCNTs have a hydrophobic surface but can exhibit a unique H_2O adsorption behavior due to the strong interaction effect between H_2O molecules and the nanotube surface. Figure 6 shows the H_2O adsorption isotherm at 303 K for the

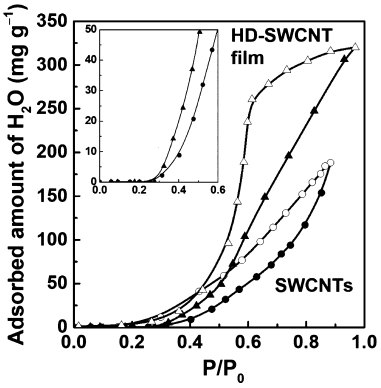

Figure 6. H_2O adsorption on the SWCNTs and the HD-SWCNT film at 303 K.

SWCNTs and the HD-SWCNT film. The H_2O adsorption of the SWCNTs is classified as IUPAC V-type with a small hysteresis, indicating that the isotherm gradually increases above P/P_0 = 0.3. The HD-SWCNT film also exhibited a similar increase at P/P_0 = 0.3 but showed a greater hysteresis than the SWCNTs, and its H_2O adsorption capacity increased significantly from 188 to 320 mg g^{-1} close to a P/P_0 value 0.9. This increased H_2O adsorption amount corresponds to a 170% greater quantity compared to that of the SWCNTs and was attributed to an increase in the number of narrow interstitial spaces measuring <0.9 nm. This result is in good agreement with previous studies showing that the amount of H_2O adsorption increases as the micropore volume of the nanohorn increases.[16] The inset in Figure 6 shows the adsorption branch of the H_2O adsorption isotherm up to P/P_0 = 0.6. In both samples, the H_2O adsorption amount increased at P/P_0 = 0.3, and the H_2O adsorption amount of the HD-SWCNT film shows a steeper rise than that of the SWCNTs.

The equilibrium time for H_2O adsorption and desorption was then determined to evaluate the H_2O adsorption rate of the HD-SWCNT film exhibiting an enhanced interstitial space. Figure 7a shows the equilibration times required for H_2O adsorption by the SWCNTs and HD-SWCNT films. More specifically, in the initial 60 min, the H_2O adsorption amounts of the SWCNTs and the HD-SWCNT film rapidly increased to 220 and 122 mg g^{-1}, respectively, prior to reaching an

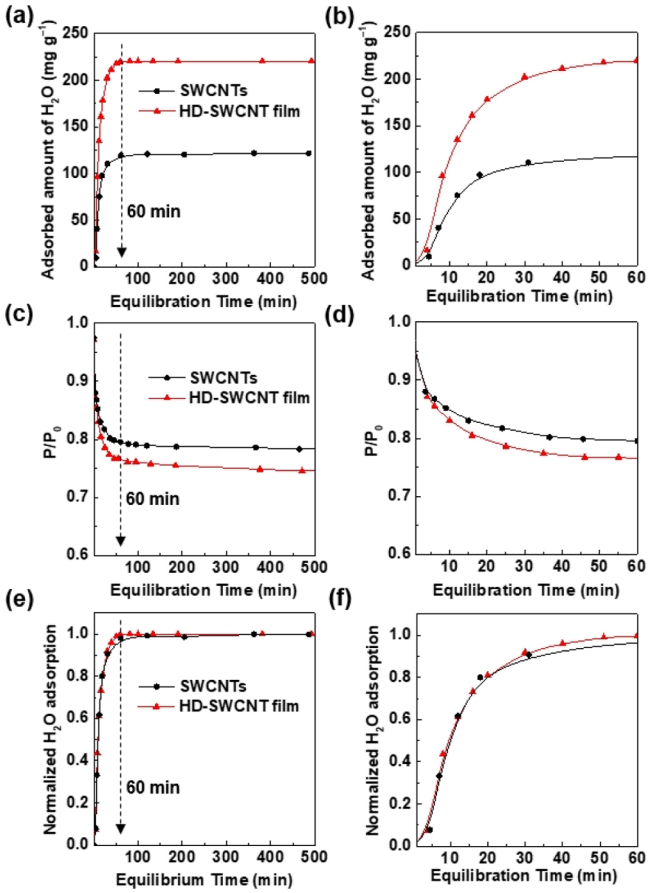

Figure 7. Effect of the equilibration time of H_2O adsorption at 303 K on the SWCNT samples. (a,b) Variation in the amount of H_2O adsorbed with equilibration time, (c,d) variation in the saturation pressure with equilibration time, and (e,f) normalization of the H_2O adsorption amount using the saturated adsorption amounts.

equilibrium state (Figure 7b). Interestingly, the adsorbed amount of H_2O was similar to the result of stepwise H_2O adsorption from a low pressure (P/P_0 = 0.005), as shown in Figure 6. In addition, Figure 7c,d shows the variations in the P/P_0 values of the SWCNTs and HD-SWCNT films. For both samples, the value of P/P_0 decreased rapidly during the initial 60 min, with an increase in the amount of H_2O adsorption being observed. Furthermore, Figure 7e,f shows the adsorption branches of the normalized H_2O adsorption rates. The larger slope observed for the normalized H_2O adsorption in this range reflects the more rapid adsorption of H_2O molecules in the narrower micropores of the interstitial space. In this system, the adsorption capacity of H_2O for the HD-SWCNT film increased by ∼180%, and the average micropore width narrowed from 1.5 to 0.9 nm; however, the slope of the adsorption rate was similar to that of the SWCNTs. This result shows that the width of the developed interstitial space in the HD-SWCNT film is not sufficiently narrow to increase the adsorption rate of H_2O. These results therefore agree with the unchanged $q_{st,\Phi=1/e}$ value of the isosteric heat value of the HD-SWCNT film during H_2 adsorption at 77 K (Table 3).

The equilibrium time for H_2O desorption was also measured, as shown in Figure 8. After H_2O adsorption by the SWCNTs and the HD-SWCNT film had reached equilibrium (i.e., after 500 min), the H_2O desorption process was performed at 303 K from P/P_0 = 0.97 to 0.001 under a

https://dx.doi.org/10.1021/acsomega.0c06302
ACS Omega 2021, 6, 7015−7022

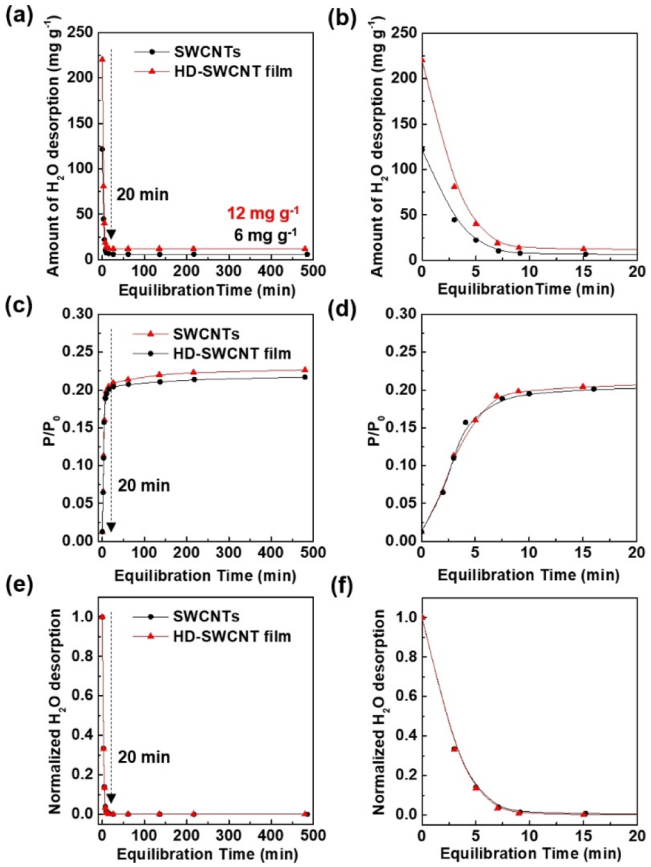

Figure 8. Effect of the equilibration time for H_2O desorption at 303 K for the SWCNTs and the HD-SWCNT film. (a,b) Variation in the amount of desorbed H_2O with equilibration time, (c,d) variation in the saturation pressure with equilibration time, and (e,f) normalization of the H_2O desorption amount using the saturated desorption amounts.

vacuum condition of 10^{-4} Pa for 500 min. Figure 8a,b shows the change in the amount of H_2O desorption on the SWCNTs and the HD-SWCNT film initiated at fully adsorbed equilibrium states. During the initial 20 min, the amount of H_2O desorption from the SWCNTs and the HD-SWCNT film decreased rapidly from 208 to 12 mg g^{-1} (~94 wt %) and from 122 to 6 mg g^{-1} (~95 wt %), respectively. Despite the intensive desorption process carried out under vacuum (10^{-4} Pa) for 500 min, ~5 wt % of the adsorbed H_2O remained in the nanopores of the SWCNTs and the HD-SWCNT film. This may be due to the high potential energy caused by the strong interactions between the nanotube surface and the H_2O molecules. Figure 8e,f shows the H_2O desorption rates for the SWCNTs and the HD-SWCNT film, whereby similar slopes can be observed for the desorption rates. These results indicate that the H_2O desorption capacity was significantly reduced, but the H_2O desorption rate did not change after introduction of the increased interstitial space in the SWCNTs upon mild HNO_3/H_2SO_4 treatment.

Finally, we summarized the relationship between the kinetic diameter and the adsorption capacities of the H_2O, H_2, CO_2, and N_2 gas molecules. More specifically, the adsorption capacities of H_2O, H_2, and CO_2 were obtained from the ratio of the increase in adsorption amount using gravimetric methods, while the value for N_2 was obtained by measuring the ratio of the total surface area, as calculated by the SPE method. Figure 9 shows that the slope corresponding to the increase in the kinetic diameter and the adsorption capacity of each

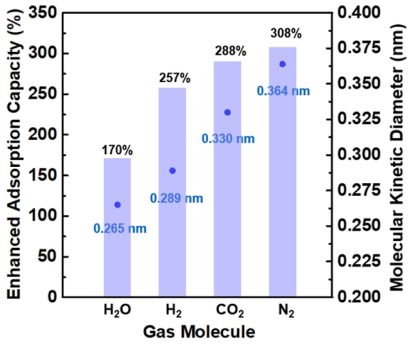

Figure 9. Relationship between the kinetic diameter and the enhanced adsorption capacities toward H_2O, H_2, CO_2, and N_2.

molecule is relatively linear, therefore indicating that the increase in the interstitial space of the SWCNTs is more appropriate for the adsorption of N_2 and CO_2 molecules (i.e., molecules with larger kinetic diameters) than H_2O molecules. Therefore, the adsorption behavior of molecules into the enhanced interstitial space is closely related to the kinetic diameter of each molecule, and as such, it is essential to properly match the interfacial engineering between the kinetic diameter and the interstitial space to maximize the adsorption capacities of gas molecules.

CONCLUSIONS

A HD-SWCNT film with a narrow interstitial space was fabricated through the mild HNO_3/H_2SO_4 treatment of SWCNTs and a subsequent VF process. The pore structure of the enhanced interstitial space of the HD-SWCNT film was analyzed by α_s-plot and DR plot analyses from the adsorption isotherms of N_2, CO_2, and H_2, which indicated a remarkably developed interstitial space with narrow micropores of an ~0.9 nm diameter. H_2O adsorption at 303 K showed that the adsorption capacity of the HD-SWCNT film increased significantly from 188 to 320 mg g^{-1}. However, in the equilibrium time measurements, despite an increase in the adsorption capacity of ~170%, the adsorption rate did not change, which indicated that the developed interstitial space had no effect on the adsorption rate of H_2O. It also shows that the adsorption behaviors of N_2, CO_2, H_2, and H_2O within the developed interstitial space are linear with respect to their kinetic diameters. This result suggests that the enhanced interstitial space of the HD-SWCNT film obtained upon mild HNO_3/H_2SO_4 treatment can provide the appropriate nanoporosity for the adsorption of larger molecules, such as N_2 and CO_2. We expect that controlling the interstitial spaces of SWCNTs through interface engineering in a scalable solution-based process will lead to their use in energy and environmental applications for selective molecular capture and also in the storage of clean fuel gases.

EXPERIMENTAL SECTION

Fabrication of the HD-SWCNT Film. SWCNTs produced by the high-pressure CO disproportionation (HiPco) process were used for the purpose of this study (Carbon Nanotechnologies, Inc., USA). The as-produced SWCNT powder was stirred in ethanol for 1 h, sonicated for 5 min, and then

https://dx.doi.org/10.1021/acsomega.0c06302
ACS Omega 2021, 6, 7015−7022

dried for 24 h at 383 K. Subsequently, the dried SWCNTs (100 mg) were stirred in a mixed solution of HNO_3 (65%) and H_2SO_4 (98%) (100 mL, 1:3 v/v) for 12 h at 298 K. The resulting acid-treated suspension was filtered through a membrane filter (10 μm pore diameter) and washed several times with distilled water. The washed sample was sonicated with distilled water for 30 min and then subjected to VF once again. The resulting HD-SWCNT film was then dried at 383 K for 24 h and annealed at 1173 K under an Ar atmosphere for 1 h.

Characterization and Gas Adsorption Experiments. The morphologies of the SWCNTs and the HD-SWCNT film were observed by FE-SEM (JEOL JSM-6330F). The chemical states of the SWCNTs and the HD-SWCNT film were analyzed by XPS (ESCALAB 250Xi, Thermo Fisher Scientific Inc.) using an Al Kα gun at 10 mA and 15 kV with a pass energy of 10 eV. A flood gun was used as a charge neutralizer. The C 1s peaks of the SWCNTs and the HD-SWCNT film were set to 284.4 eV for calibrating the binding energy values. All C 1s spectra were normalized by adjusting the maximum intensities of the C 1s spectra to 1.0. The pore structures of the SWCNT samples were analyzed from the adsorption isotherms of N_2 (77 K), CO_2 (273 K), and H_2 (77 K) using volumetric equipment (Quantachrome AS-1-MP) after preheating at 423 K under 10^{-4} Pa for 2 h. The parameters of the pore structures were calculated by the SPE method and the DR method. The SPE method was derived using high-resolution α_s-plots constructed for standard adsorption data for highly crystalline non-porous carbon black.[44] The adsorption isotherms of H_2O in the SWCNTs and the HD-SWCNT film were measured gravimetrically at 303 K after prevacuum treatment at 10^{-4} Pa and 423 K for 2 h. H_2O was introduced into the adsorption cell after repeated purification via freeze−pump−thaw cycling. For the H_2O adsorption and desorption equilibrium time measurements of the SWCNT samples, distilled water was injected at a pressure P/P_0 of ∼0.97 (corresponding to an equivalent H_2O vaporization of 31.8 Torr at 303 K) after pre-evacuation at 423 K and 10^{-4} Pa for 2 h. The changes in the adsorption amount and in P/P_0 with the equilibrium time were recorded.

AUTHOR INFORMATION

Corresponding Authors

Dong Young Kim − *Department of Applied Chemistry, Waseda University, Tokyo 169-8555, Japan*; Email: dykim2100@gmail.com

Jungpil Kim − *Carbon Materials Application Research Group, Korea Institute of Industrial Technology (KITECH), Jeonju 54853, Korea*; orcid.org/0000-0003-3663-2774; Phone: +82-63-210-3714; Email: jpkim@kitech.re.kr; Fax: +82-63-210-3714

Authors

Keun Soo Kim − *Department of Physics and Astronomy, Sejong University, Seoul 05006, Republic of Korea*; orcid.org/0000-0002-4901-6156

Cheol-Min Yang − *Institute of Advanced Composite Materials, Korea Institute of Science and Technology (KIST), Wanju-gun, Jeonbuk 55324, Korea*; orcid.org/0000-0001-9698-6684

Complete contact information is available at: https://pubs.acs.org/10.1021/acsomega.0c06302

Notes

The authors declare no competing financial interest.

ACKNOWLEDGMENTS

This work was supported by the Korea Institute of Industrial Technology.

REFERENCES

(1) da Silva, A.; Donoso, P.; Aegerter, M. A. Properties of water adsorbed in porous silica aerogels. *J. Non-Cryst. Solids* **1992**, *145*, 168−174.

(2) Yanagihara, H.; Yamashita, K.; Endo, A.; Daiguji, H. Adsorption−desorption and transport of water in two-dimensional hexagonal mesoporous silica. *J. Phys. Chem. C* **2013**, *117*, 21795−21802.

(3) Wade, C. R.; Corrales-Sanchez, T.; Narayan, T. C.; Dincă, M. Postsynthetic tuning of hydrophilicity in pyrazolate MOFs to modulate water adsorption properties. *Energy Environ. Sci.* **2013**, *6*, 2172−2177.

(4) Furukawa, H.; Gándara, F.; Zhang, Y.-B.; Jiang, J.; Queen, W. L.; Hudson, M. R.; Yaghi, O. M. Water adsorption in porous metal-organic frameworks and related materials. *J. Am. Chem. Soc.* **2014**, *136*, 4369−4381.

(5) Hwang, J.; Kataoka, S.; Endo, A.; Daiguji, H. Adsorption and desorption of water in two-dimensional hexagonal mesoporous silica with different pore dimensions. *J. Phys. Chem. C* **2015**, *119*, 26171−26182.

(6) Ghosh, S.; Hariharan, S.; Tiwari, A. K. Water adsorption and dissociation on copper/nickel bimetallic surface alloys: effect of surface temperature on reactivity. *J. Phys. Chem. C* **2017**, *121*, 16351−16365.

(7) Bucher, D.; Kuyucak, S. Importance of water polarization for ion permeation in narrow pores. *Chem. Phys. Lett.* **2009**, *477*, 207−210.

(8) Sakamoto, T.; Ogawa, T.; Nada, H.; Nakatsuji, K.; Mitani, M.; Soberats, B.; Kawata, K.; Yoshio, M.; Tomioka, H.; Sasaki, T.; Kimura, M.; Henmi, M.; Kato, T. Development of nanostructured water treatment membranes based on thermotropic liquid crystals: Molecular design of sub-nanoporous materials. *Adv. Sci.* **2018**, *5*, 1700405.

(9) Cohen-Tanugi, D.; Grossman, J. C. Water desalination across nanoporous graphene. *Nano Lett.* **2012**, *12*, 3602−3608.

(10) Kou, J.; Yao, J.; Wu, L.; Zhou, X.; Lu, H.; Wu, F.; Fan, J. Nanoporous two-dimensional MoS_2 membranes for fast saline solution purification. *Phys. Chem. Chem. Phys.* **2016**, *18*, 22210−22216.

(11) Hanzawa, Y.; Kaneko, K. Lack of a predominant adsorption of water vapor on carbon mesopores. *Langmuir* **1997**, *13*, 5802−5804.

(12) Kaneko, K.; Hanzawa, Y.; Iiyama, T.; Kanda, T.; Suzuki, T. Cluster-mediated water adsorption on carbon nanopores. *Adsorption* **1999**, *5*, 7−13.

(13) Ohba, T.; Kanoh, H.; Kaneko, K. Cluster-growth-induced water adsorption in hydrophobic carbon nanopores. *J. Phys. Chem. B* **2004**, *108*, 14964−14969.

(14) Liu, L.; Tan, S. J.; Horikawa, T.; Do, D. D.; Nicholson, D.; Liu, J. Water adsorption on carbon - A review. *Adv. Colloid Interface Sci.* **2017**, *250*, 64−78.

(15) Ito, H.; Vallejos-Burgos, F.; Ono, Y.; Yoshimoto, M.; Kaneko, K.; Futamura, R.; Iiyama, T.; Matsumoto, A. Isotope effect on adsorption diffusivity of water molecules in hydrophobic carbon micropores. *Carbon* **2020**, *168*, 415−418.

(16) Pina-Salazar, E. Z.; Kaneko, K. Adsorption of water vapor on mesoporosity-controlled singe wall carbon nanohorn. *Colloid Interface Sci. Commun.* **2015**, *5*, 8−11.

(17) Chairunnisa; Mikšík, F.; Miyazaki, T.; Thu, K.; Miyawaki, J.; Nakabayashi, K.; Wijayanta, A. T.; Rahmawati, F. Enhancing water adsorption capacity of acorn nutshell based activated carbon for adsorption thermal energy storage application. *Energy Rep.* **2020**, *6*, 255−263.

(18) Yang, C.-M.; Kaneko, K. Adsorption properties of iodine-doped activated carbon fiber. *J. Colloid Interface Sci.* **2002**, *246*, 34−39.
(19) Ohba, T.; Kanoh, H.; Kaneko, K. Affinity transformation from hydrophilicity to hydrophobicity of water molecules on the basis of adsorption of water in graphitic nanopores. *J. Am. Chem. Soc.* **2004**, *126*, 1560−1562.
(20) Kaneko, K. Water capture in carbon cuboids. *Nat. Chem.* **2015**, *7*, 194−196.
(21) Hiraoka, T.; Izadi-Najafabadi, A.; Yamada, T.; Futaba, D. N.; Yasuda, S.; Tanaike, O.; Hatori, H.; Yumura, M.; Iijima, S.; Hata, K. Compact and light supercapacitor electrodes from a surface-only solid by opened carbon nanotubes with 2200 m^2 g^{-1} surface area. *Adv. Funct. Mater.* **2010**, *20*, 422−428.
(22) Chen, Z.; Kim, D. Y.; Hasegawa, K.; Noda, S. Methane-assisted chemical vapor deposition yielding millimeter-tall single-wall carbon nanotubes of smaller diameter. *ACS Nano* **2013**, *7*, 6719−6728.
(23) Hummer, G.; Rasaiah, J. C.; Noworyta, J. P. Water conduction through the hydrophobic channel of a carbon nanotube. *Nature* **2001**, *414*, 188−190.
(24) Holt, J. K.; Park, H. G.; Wang, Y.; Stadermann, M.; Artyukhin, A. B.; Grigoropoulos, C. P.; Noy, A.; Bakajin, O. Fast mass transport through sub-2-nanometer carbon nanotubes. *Science* **2006**, *312*, 1034−1037.
(25) Joseph, S.; Aluru, N. R. Why are carbon nanotubes fast transporters of water? *Nano Lett.* **2008**, *8*, 452−458.
(26) Kipper, A. C.; da Silva, L. B. Water filling of carbon nanotubes membranes: Porosity and temperature effects. *Chem. Phys. Lett.* **2012**, *552*, 84−87.
(27) Tunuguntla, R. H.; Henley, R. Y.; Yao, Y.-C.; Pham, T. A.; Wanunu, M. Enhanced water permeability and tunable ion selectivity in subnanometer carbon nanotube porins. *Science* **2017**, *357*, 792−796.
(28) Ohba, T. Size-dependent water structures in carbon nanotubes. *Angew. Chem., Int. Ed.* **2014**, *53*, 8032−8036.
(29) Ohba, T.; Taira, S.-i.; Hata, K.; Kanoh, H. Mechanism of sequential water transportation by water loading and release in single-walled carbon nanotubes. *J. Phys. Chem. Lett.* **2013**, *4*, 1211−1215.
(30) Wang, H.-J.; Xi, X.-K.; Kleinhammes, A.; Wu, Y. Temperature-induced hydrophobic-hydrophilic transition observed by water adsorption. *Science* **2008**, *322*, 80−83.
(31) Lee, B.; Baek, Y.; Lee, M.; Jeong, D. H.; Lee, H. H.; Yoon, J.; Kim, Y. H. A carbon nanotube wall membrane for water treatment. *Nat. Commun.* **2015**, *6*, 7109.
(32) Hassan, J.; Diamantopoulos, G.; Homouz, D.; Papavassiliou, G. Water inside carbon nanotubes: Structure and dynamics. *Nanotechnol. Rev.* **2016**, *5*, 341−354.
(33) Yang, C.-M.; Kaneko, K.; Yudasaka, M.; Iijima, S. Effect of purification on pore structure of HiPco single-walled carbon nanotube aggregates. *Nano Lett.* **2002**, *2*, 385−388.
(34) Yang, C.-M.; Kim, D. Y.; Lee, Y. H. Formation of densely packed single-walled carbon nanotube assembly. *Chem. Mater.* **2005**, *17*, 6422−6429.
(35) Landi, B. J.; Ganter, M. J.; Schauerman, C. M.; Cress, C. D.; Raffaelle, R. P. Lithium ion capacity of single wall carbon nanotube paper electrodes. *J. Phys. Chem. C* **2008**, *112*, 7509−7515.
(36) Kim, D. Y.; Yang, C.-M.; Yamamoto, M.; Lee, D. H.; Hattori, Y.; Takahashi, K.; Kanoh, H.; Kaneko, K. Supercritical hydrogen adsorption of ultramicropore-enriched single-wall carbon nanotube sheet. *J. Phys. Chem. C* **2007**, *111*, 17448−17450.
(37) Kim, D. Y.; Yang, C.-M.; Noguchi, H.; Yamamoto, M.; Ohba, T.; Kanoh, H.; Kaneko, K. Enhancement of H_2 and CH_4 adsorptivities of single wall carbon nanotubes produced by mixed acid treatment. *Carbon* **2008**, *46*, 611−617.
(38) Niu, Z.; Zhou, W.; Chen, J.; Feng, G.; Li, H.; Ma, W.; Li, J.; Dong, H.; Ren, Y.; Zhao, D.; Xie, S. Compact-designed super-capacitors using free-standing single-walled carbon nanotube films. *Energy Environ. Sci.* **2011**, *4*, 1440−1446.
(39) Kim, J.; Yamada, Y.; Suzuki, Y.; Ciston, J.; Sato, S. Pyrolysis of epoxidized fullerenes analyzed by spectroscopies. *J. Phys. Chem. C* **2014**, *118*, 7076−7084.
(40) Yamada, Y.; Yasuda, H.; Murota, K.; Nakamura, M.; Sodesawa, T.; Sato, S. Analysis of heat-treated graphite oxide by X-ray photoelectron spectroscopy. *J. Mater. Sci.* **2013**, *48*, 8171−8198.
(41) Kim, J.; Lee, N.; Min, Y. H.; Noh, S.; Kim, N.-K.; Jung, S.; Joo, M.; Yamada, Y. Distinguishing zigzag and armchair edges on graphene nanoribbons by X-ray photoelectron and Raman spectroscopies. *ACS Omega* **2018**, *3*, 17789−17796.
(42) Kim, J.; Yamada, Y.; Kawai, M.; Tanabe, T.; Sato, S. Spectral change of simulated X-ray photoelectron spectroscopy from graphene to fullerene. *J. Mater. Sci.* **2015**, *50*, 6739−6747.
(43) Kim, J.; Han, J.-W.; Yamada, Y. Heptagons in the basal plane of graphene nanoflakes analyzed by simulated X-ray photoelectron spectroscopy. *ACS Omega* **2021**, *6*, 2389−2395 , in press.
(44) Ohba, T.; Kaneko, K. Internal surface area evaluation of carbon nanotube with GCMC simulation-assisted N_2 adsorption. *J. Phys. Chem. B* **2002**, *106*, 7171−7176.
(45) Mehio, N.; Dai, S.; Jiang, D.-e. Quantum mechanical basis for kinetic diameters of small gaseous molecules. *J. Phys. Chem. A* **2014**, *118*, 1150−1154.
(46) Luo, Y.; Funke, H. H.; Falconer, J. L.; Noble, R. D. Adsorption of CO_2, CH_4, C_3H_8, and H_2O in SSZ-13, SAPO-34, and T Type Zeolites. *Ind. Eng. Chem. Res.* **2016**, *55*, 9749−9757.
(47) Kaneko, K. Effect of temperature on micropore filling of supercritical NO on Fe_2O_3-dispersed activated carbon fibers. *Colloids Surf.* **1989**, *37*, 115−124.
(48) Kaneko, K.; Murata, K.; Shimizu, K.; Camara, S.; Suzuki, T. Enhancement effect of micropore filling for supercritical methane by magnesia dispersion. *Langmuir* **1993**, *9*, 1165−1167.
(49) Kaneko, K.; Murata, K. An analytical method of micropore filling of a supercritical gas. *Adsorption* **1997**, *3*, 197−208.

https://dx.doi.org/10.1021/acsomega.0c06302
ACS Omega 2021, 6, 7015−7022